Simple liquids confined to molecularly thin layers. I. Confinement-induced liquid-to-solid phase transitions

Jacob Klein[a] and Eugenia Kumacheva[b]
Weizmann Institute of Science, Rehovot 76100, Israel

(Received 2 September 1997; accepted 14 January 1998)

A surface force balance with extremely high resolution in measuring shear forces has been used to study the properties of films of the simple organic solvents cyclohexane, octamethylcyclotetrasiloxane, and toluene, confined in a gap between smooth solid surfaces. We were able to probe in detail the transition between liquidlike and solidlike behavior of the films as the gap thickness decreased. Our results reveal that in such confined layers the liquids are fluid down to a film thickness of few molecular layers (typically seven, depending on the particular liquid examined). On further decreasing the gap thickness by a single molecular layer, the films undergo an abrupt transition to become solidlike in the sense that they are able to sustain a finite shear stress for macroscopic times. At the transition, the effective rigidity of the films, quantified in terms of an effective creep viscosity, increases by at least seven orders of magnitude. This sharp transition is reversible and occurs as a function of the confinement alone: it does not require external applied pressure. Following the transition the confined films behave under shear in a manner resembling ductile solids. © *1998 American Institute of Physics.* [S0021-9606(98)51415-8]

I. INTRODUCTION

In recent years the properties of simple liquids in the vicinity of solid surfaces, both for bulk liquids and particularly when they are confined to thin films, have been studied extensively. This is partly because of obvious practical connections (friction and lubrication,[1] wetting properties,[2] adhesion and wear[3,4]), but at the same time because the behavior of liquids in ultrathin films is not yet well understood. An outstanding issue, on which we shall focus in this paper, concerns the manner in which liquid films change from being fluid in macroscopically thick films, to behaving like solids when confined to films only a monolayer or two in thickness.[1,5–7] For bulk liquids in contact with a single smooth solid surface, layering of the molecules is induced, decaying over a few molecular diameters from the surface.[8–10] The question of the fluidity of liquids near a surface has also been examined.[8,9] Careful determinations of the plane of zero shear when liquids flow past a single solid surface indicate that bulk simple liquids near a surface remain fluid right up to the solid–liquid interface.[11–13] Surface force balances (SFB) have been used to probe both the dynamic and the structural properties of ultrathin films and suggest that, even when confined, liquids retain their bulk viscosity as long as the films are thicker than about ten molecular diameters.[11–14] At the other extreme, highly compressed films of simple liquids confined to 1–3 molecular layers between smooth solid surfaces have been shown to display solidlike features, manifested by a finite yield stress[5,6,15,16] and characteristic stick-slip behavior,[1] as well as a marked layering of the confined molecules.[17,18]

Few experimental studies have addressed the process by which a liquid changes to a solid as it becomes confined to increasingly smaller gaps. Some studies based on the shear of highly compressed layers between parallel plates have reported that these undergo a continuous increase in their viscosity as the plate separation decreases below a few nanometers.[19–21] This regime has been described as ''intermediate'' between a bulk liquid and a solid, and it has been remarked[19,20] that the effective viscosity η_{eff} of some liquids in this regime varies with the shear rate $\dot{\gamma}$ as $\eta_{\mathrm{eff}} \propto \dot{\gamma}^{-2/3}$. In contrast, a different picture, where the liquid-to-solid transition in simple liquids is a very sharp one and occurs on increasing confinement at a well-defined film thickness, with no intermediate regime, has recently been reported.[7]

Computer simulations and theoretical investigations have shed much light on the molecular details underlying both structural and dynamic behavior of liquids in the highly confined regime, as will be discussed in more detail later. Several studies suggest that liquids composed of spherical molecules may undergo a sharp liquid-to-solid transition on confinement to a few monolayers.[22–27] In others, the variation of liquid viscosity with shear rate in ultrathin confined films is explored, as is the question of stick-slip sliding between the confining surfaces.[25,26,28–30] Very recently, the nature of the confinement-induced liquid-to-solid transition itself has been addressed directly both analytically[31,32] and via computer simulation studies.[27,33]

The present study extends our earlier brief report of confinement-induced phase transitions in a simple liquid.[7] Using a surface force balance with uniquely high resolution in directly measuring shear forces across thin films, we investigate a number of simple nonpolar liquids with quasi-spherical molecules, and examine comprehensively the dynamical and mechanical behavior of the confined films. Our

[a]Author to whom correspondence should be addressed.
[b]Present address: Department of Chemistry, University of Toronto, Toronto, ON M5S 3H6, Canada.

study reveals several qualitatively new features of thin-film properties. In this first paper (I) we focus on the issue of the transition in the behavior of the confined films as the film thickness is reduced from macroscopic dimensions to the point where the liquid behaves in a solidlike fashion. In Sec. II we describe in detail the surface force balance and its operation. The effect of increasing confinement on the shear response of the liquids is described in Sec. III. In the final section we consider this behavior in the light of theoretical and computer simulation studies, as well as of earlier investigations on confined simple liquids. In the following paper (II) we report on the properties of the solidlike confined films, that is, after they have undergone the liquid-to-solid transition.

II. EXPERIMENT

A. Apparatus and measurements

The use of mica as a model smooth substrate to measure friction was first reported by Bailey and Courtney-Pratt[34] who deposited boundary lubricants on the mica surfaces. Surface force balances (SFB), where normal forces between atomically smooth, curved mica surfaces are directly measured as a function of their separation, have been utilized extensively since their first descriptions in the late 1960s by Tabor and co-workers,[35] and especially following their extension by Israelachvili and Adams to the case of forces across liquid media.[36] Force balances have also been used to investigate friction and shear forces across mica sheets, between which different materials (such as polymers, surfactants, or simple liquids) could be compressed.[5,6,37–40] In our previous investigations we examined the shear forces between polymer-bearing mica surfaces (both adsorbed and end-tethered chains) immersed in a solvent.[40–42] Due to the remarkable lubricating properties of polymer brushes in good solvents, the shear forces during steady sliding, even under substantial normal loads, can be several orders of magnitude weaker than the smallest forces measureable with earlier force balances. The apparatus used in the present study was originally designed to measure these very weak forces.

Figure 1 shows the surface force balance schematically (a brief description has appeared earlier[40]). The normal forces $F(D)$ and lateral (or shear) forces $F_s(D)$ between the two curved mica sheets a closest distance D apart are measured by monitoring the bending of two orthogonal sets of leaf springs, vertical springs S_1 (spring constant $K_1 = 300$ N/m), and a horizontal spring S_2 (spring constant $K_2 = 150$ N/m). The bending of S_2 (on which the lower mica surface is mounted) is determined, as in earlier versions,[35,36,43] using multiple beam interferometry. This is done by monitoring the change in wavelength of fringes of equal chromatic order (FECO) in response to applied motion in the z direction.

Application of shear motion and measurements of the shear force are carried out as follows. The top mica surface is mounted on a piezoelectric tube (PZT, diameter 12.7 mm, length 12.7 mm, and wall thickness ca. 1 mm, ceramic material 5-H, supplied by Morgan Matroc Ltd., UK, cat. no. 8531-5H) whose outside silvered surface is divided, by removal of four narrow conducting strips at 90° intervals, into four equal sectors $A-D$. By applying equal and opposite voltages (with respect to the inner conducting surface E of the PZT) to two of the opposing outside sectors (say A and C which oppose each other along x in Fig. 1), one expands while the other contracts. This provides a lateral motion (in the x direction) to the top mica surface, as indicated in the right of Fig. 1. The range of lateral motion is some 15 000 Å in either the $+x$ or $-x$ directions, for a total lateral motion amplitude $x_m \approx 30\,000$ Å. The resonance frequency of the PZT in its shear mode is over 100 kHz, but in the configuration shown in Fig. 1 the maximum usable shear frequency ν_m is limited by the mounting BO to $\nu_m \approx 550$ Hz. The full range of accessible mean shear velocities v_s is thus from rest ($v_s = 0$) to a maximal value $v_s = 2x_m\nu_m \approx 3.5\times 10^7$ Å/s (a steplike voltage pulse can result in even higher instantaneous shear velocities). Any shear forces acting between the top and bottom mica surfaces, as the former are made to move in the x direction, are transmitted to the vertical springs S_1 via the rigid stainless steel mount BO on which the top surface is mounted (the total mass of the PZT and upper lens and the boat BO on which they are mounted is ca. 20 g).[44]

The sectored PZT is especially versatile in providing both shear and normal motion of the upper mica surface: pure normal motion (in the z direction) occurs when the potentials of all four outer sectors are equal. A change in this potential then produces pure axial extension or contraction: this is used particularly for the measurement of the profiles of normal interactions between the surfaces. The PZT can

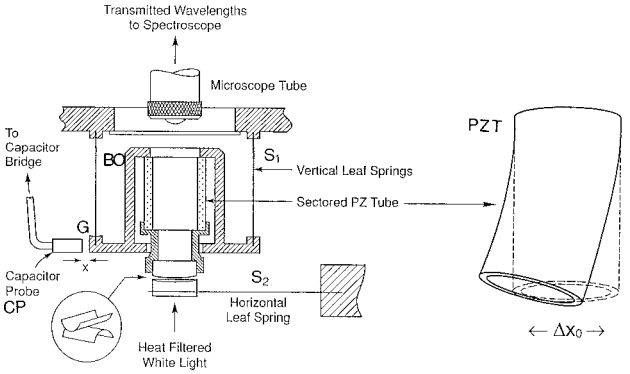

FIG. 1. Schematic (approximately to scale) of the shear force balance used in the present experiments. The two mica sheets are mounted on cylindrical quartz lenses in a crossed-cylinder configuration (inset). The top lens is mounted on a sectored piezoelectric tube (PZT, shown blown up on the right and illustrating the sideways motion induced when opposing sectors in the x-direction experience equal and opposite potentials). The PZT (see text for specifications) is mounted via a rigid stainless steel boat BO onto two vertical copper-berrylium leaf springs S_1 (spring constant $K_1 = 300$ N/m) which are rigidly mounted into the main body of the balance. Lateral forces between the mica surfaces are transmitted to the springs S_1, whose bending changes the thickness x of the air-gap G between the boat BO and a capacitance probe CP. This is monitored by the change in capacitance of G (measured with a capacitor bridge, see text for details). Normal forces are measured via the bending of the horizontal stainless steel leaf spring S_2 (spring constant $K_2 = 150$ N/m), whose motion is a perfect up–down one without tilt (the single cantilever representation of S_2 is for simplicity). The distance D between the mica surfaces is measured as usual via the fringes of equal chromatic order origination from the white light after projection onto the slit of the spectroscope.

also provide simultaneous normal and shear motion, by independent adjustment of the voltages applied to the inner and outer sectors (E and $A-D$, respectively), which enables measurement of shear forces while very delicately varying the normal forces. In addition, it can provide motion of any desired form in the x-y plane (not only along x) by suitable synchronized inputs to the four sectors (for example, motion at 45° to x, at right angles to x, i.e. along y, or circular motion in the x-y plane). This can be especially revealing where the shear forces are anisotropic with respect to the relative shear direction, as in the case of confined liquid crystals.[45] In the present experiments only motion along x was utilized.

The bending of S_1 in response to the shear forces is detected by the changes in the capacitance of a small gap G between a fixed capacitance probe CP and the moving boat BO as shown. The capacitance bridge (Accumeasure 1000, probe ASP-1-ILA, MTI Ltd., Albany, NY) can detect changes δx in the gap G as low as $\delta x = \pm 2$ to 3 Å, providing an optimal sensitivity $K_1 \delta x$ of better than ± 0.1 μN in measuring $F_s(D)$. These values of the sensitivity and resolution in measuring the shear forces in monotonic sliding motion are comparable to those achievable in measuring the normal forces $F(D)$. They are about 100–1000 times better than values reported in earlier studies[5,6,15] where frictional forces were measured between mica surfaces sliding steadily past each other across simple liquids. Such sensitivity is essential for the measurement of the weak shear forces reported in the present study (and, particularly, for measuring the ultraweak shear forces between sliding polymer brushes reported earlier[41]). The actual output of the capacitance bridge is in volts, linear in the dimensions of the capacitance gap G; it is calibrated in the factory (1 mV=25.0 Å) and checked by us prior to each experiment (see below). In an experiment, following mounting of the surfaces, the capacitor gap G is adjusted to be parallel, and set, using a differential micrometer (not shown in Fig. 1), to the appropriate dimensions, within the thickness range 20 ± 10 μm.

Random vibrations due to ambient noise are minimized by a custom-built electronic vibration isolation unit specially tuned to eliminate the low-frequency tilting motion of the building (MOD 2A, JRS Ltd, Zurich). All experiments were carried out at 23.5 °C. The rooms in which experiments were performed were thermally insulated and actively temperature controlled to ± 0.25 °C in order to minimize thermal drift.

A central requirement in measuring the shear forces is that the surfaces move parallel to each other, at any given separation D, when lateral motion is applied to the top surface. This is because changes in D can lead to rapid changes in the normal force, which in turn result in changes in $F_s(D)$. In general it is not possible to ensure that mechanical mounting of the PZT, boat BO, and springs S_1 will result in completely parallel motion of the surfaces when they are not in contact with each other under strong compression. To correct for this, a small proportion of the voltage applied to either sector A or sector C of the PZT (when A and C are the active sectors) is fed back to the inner sector E. Since the voltage on sector E provides for pure axial extension or contraction (z direction) of the PZT, independent of the shear motion, the adjustable feedback enables elimination of any changes in the surface separation D, even when the surfaces are not in contact, when the top surface is moved laterally. In practice, it is possible to ensure that D changes by no more than ca. 10 Å as the top surface traverses the entire range of lateral motion of 30 000 Å. Over the more usual range of lateral motion in the experiments of order 10^3 Å, the changes in D during the lateral motion can be adjusted to be less than 1 Å. At the same time, the extent of tilt due to the cantilever motion of the PZT is extremely small, corresponding to a change in D of less than 1 Å for a lateral motion of 10^4 Å of the top surface.

In a shear experiment, in addition to measuring the distance D and the normal force $F(D)$ between the surfaces, two additional outputs are recorded simultaneously. These are the voltage applied to the PZT, which gives a direct measure of the applied lateral motion, and the signal from the capacitor bridge, which monitors the bending of the vertical springs S_1, and thereby provides a direct measure of the shear force F_s. These are recorded simultaneously either on an XYt double pen chart recorder or via a storage oscilloscope. In the latter case signal averaging is possible (if desired) to enhance the signal-to-noise level. In Fig. 2 we illustrate typical outputs from the surface force balance.

In Fig. 2(a) the surfaces are in contact with no lateral motion applied to the top surface. The level of this null signal, trace 2(a) (from the capacitor bridge), is a measure of the sensitivity and resolution to which forces may be measured: as noted, the noise level δx sets this resolution at $K_1 \delta x \approx \pm 0.1$ μN. When the surfaces are far from contact the noise level can be larger (examples are given later). Trace 2(b) shows the voltage applied to the PZT when a back-and-forth shear motion Δx_0 is applied to the top surface: here the surfaces are in adhesive contact (in air), and trace 2(c) shows the bending Δx of the vertical springs in response to the shear force between them. Whenever this shear force $K_1 \Delta x$ is less than the frictional force between the surfaces, they move together, as shown in trace 2(c). That is, $\Delta x = \Delta x_0$. (This type of measurement is carried out in each experiment to calibrate the shear motion.)

Finally, trace 2(d) shows the shear response when the shear force $K_1 \Delta x$ exceeds the frictional force. In this example, four monolayers of cyclohexane are confined between the surfaces: the surfaces adhere and move together as long as the shear force is less than the static friction force between them. When the shear force $K_1 \Delta x$ exceeds the static friction they slide via a characteristic stick-slip motion. This type of motion occurs when the confined material, which is able to sustain a finite shear stress, breaks down at some critical value of the increasing stress, at the top of the spikes indicated by C in Fig. 2(d). The surfaces then slide or slip rapidly relative to each other to relieve some of the stress, as in the vertical portions following the spike tips, but at some finite shear stress, as shown by point D in Fig. 2(d), they stick together again. The confined material is then once more capable of sustaining a shear stress, and the cycle repeats itself. We note especially in Fig. 2(d) the very high reproducibility of the stick-slip pattern between consecutive back-and-forth sliding cycles.

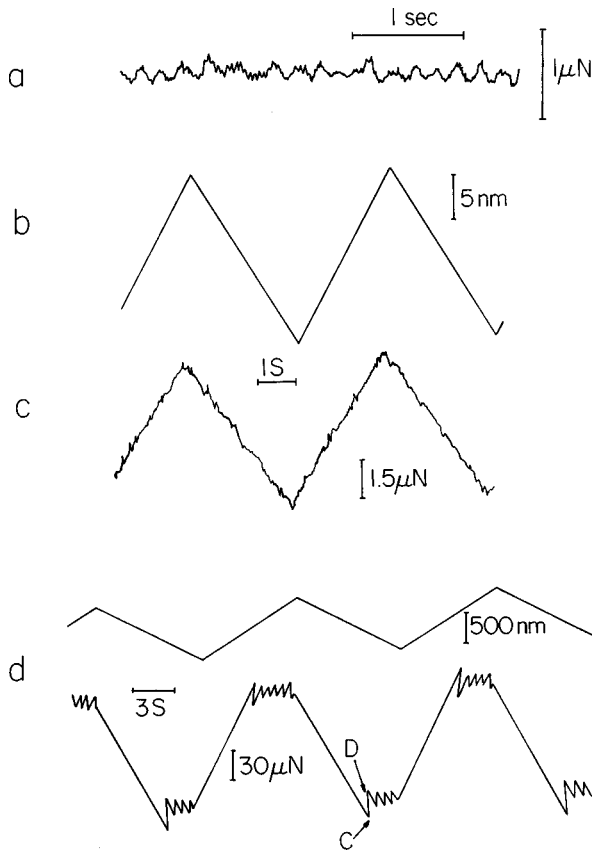

FIG. 2. Traces corresponding to typical output of the shear experiment. (a) Variation with time of the capacitor bridge signal (corresponding to the bending of the vertical leaf springs S_1), giving the equivalent shear force between the upper and lower surfaces, when the two are in adhesive contact in air. No lateral motion is applied to the top surface. (b) Variation with time of the voltage applied to the sectored PZT, giving the back-and-forth lateral motion of the upper surface. (c) Variation of the shear force between the surfaces (derived from the changes in capacitor bridge signal) corresponding to the applied motion in (b) when the surfaces are in adhesive air contact. The frictional force exceeds the shear force at all points and the surfaces move together without sliding. (d) Upper trace: applied back-and-forth motion of the upper surface. Lower trace: corresponding variation of the shear force between the surfaces, separated by $n=4$ layers of cyclohexane under a normal load $F/R=3.5$ mN/m. When the shear force exceeds the frictional force slip occurs between the surfaces (e.g., at point C to point D) which then stick together again (at point D) when the stress has partially relaxed.

B. Materials

Three different liquids were examined: cyclohexane, toluene, and octamethylcyclotetrasiloxane (OMCTS). Both cyclohexane and OMCTS, especially the latter, due to its nonpolar nature and the large size of its quasispherical molecules (diameter ca. 9 Å), have been used as model liquids in several earlier investigations.[15–17,20,21] Their structures, molecular dimensions, and melting temperatures are given in Table I.

Analytical grade toluene (Fluka) was used as received from freshly opened bottles. Cyclohexane (Fluka, analytical grade) and OMCTS (Fluka, purum grade, 99% pure) were stored for 2 days above 4A molecular sieves and then distilled over pure, dry, filtered nitrogen. In several of the experiments the liquids were twice distilled over nitrogen. For OMCTS the middle fraction boiling at 175 °C (the literature boiling temperature) was collected, and injected into the bath of the force balance (Fig. 1) under dry filtered nitrogen. The inside of the force balance was kept dry with P_2O_5. We found that for cyclohexane this distillation procedure did not result in noticeable changes relative to using cyclohexane directly from a freshly opened bottle, and in a number of the experiments this latter procedure was used. For the case of OMCTS, however, we found that distillation and transfer of the liquid under dry nitrogen to a balance in which a dry atmosphere was maintained influenced the value of structural forces, and were essential for observing the behavior under confinement described in this report.

All organic liquids used to clean the apparatus were analytical grade. Water used was purified (ELGA-Q water purification system). Sym(diphenyl carbazide) was used to glue the mica sheets to the cylindrical glass lenses for the cyclohexane and OMCTS experiments, and sucrose was used as the glue for the toluene experiments (both glues were BDH analytical grade).

Results shown are from several different experiments, with data often taken from a number of different contact points between the mica surfaces in each experiment.

III. RESULTS

A. Normal force profiles

Prior to shear measurements the normal force profiles $F(D)$ were determined in each experiment. Figures 3 and 4 show typical normalized force-distance profiles for cyclohexane and for OMCTS. The profiles show characteristic oscillations, with each maximum corresponding to a discrete number n of monolayers, as marked. They are closely similar to those reported earlier for these liquids (see captions to Figs. 3 and 4, and also Fig. 5). The issue of sample purity is crucial, as impurities can result in partial or total suppression of the structural oscillations (especially if the impurities are surface active) and, as we see later, in strong modification of the shear behavior of the confined liquids. In Fig. 5 our data for the structural oscillations in OMCTS are compared with several independent earlier determinations[17,46–48] of structural forces in this liquid which had been purified and distilled or double distilled in a similar manner to that in the present study. While there is appreciable scatter, for reasons which have been discussed,[48] nonetheless data from all such studies fall within the shaded bands indicated.[49] In contrast, where the OMCTS is not distilled, the magnitudes of the repulsive structural forces are very much weaker (open circles in Fig. 5), presumably because of the presence of foreign (non-OMCTS) molecules.[50] Studies on OMCTS where the effect of added foreign molecules or of slight roughening of the confining surfaces has been explicitly investigated[46,47,51] also show a much reduced magnitude of the structural forces. Taken together, these observations unambiguously show that the effect of foreign molecules is to disrupt the ordering/layering of the molecules of the confined OMCTS, and that in order to eliminate such a disruption it is important to distil carefully the as-received liquid as well as to dry it thoroughly. Determination of the oscillatory force profiles at the beginning of each experiment was thus a pre-

TABLE I. Structure and properties of liquids used.

Liquid	Structure and formula	Approximate diameter (Å)	Melting temp. (°C)
Octamethylcyclo-tetrasiloxane (OMCTS)	$(SiO)_4(CH_3)_8$ 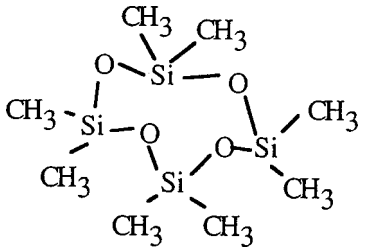	8.5–9	17
Cyclohexane	C_6H_{12} 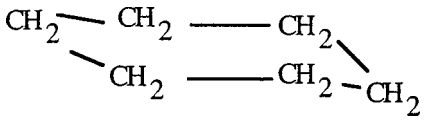	5.5	6
Toluene	$C_6H_5CH_3$ 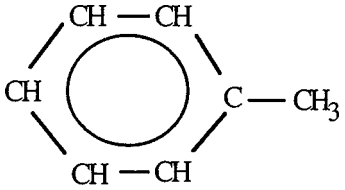	(6)	−95

condition for its continuation, as absence or reduced magnitude of the oscillations generally indicated the presence of impurities.[52]

Similar oscillations could be observed for toluene, though these could be observed to some four or five layers only, and were not accurately measured in this study. Oscillations were monitored frequently during the course of an experiment for control of its continuing integrity. At the highest normal compressions applied in this study the liquids were squeezed down to $n=3$ layers, though on occasion, when sheared at high compressions, a further layer could be ''squeezed out'', to $n=2$. At the highest compressions we were able to observe some flattening of the surfaces near the contact region (see below).

B. Confinement-induced liquid-to-solid transitions

We discovered that on progressively bringing the surfaces closer together, we could induce, by increased confinement alone, sharp transitions in the dynamic properties of the liquids in the gap. Figure 6 shows a qualitative manifestation of the sharpness of this transition (for the case of OMCTS) as the two mica surfaces approach. The traces shown record directly the change in capacitance of the air gap G (Fig. 1), and thus monitor the variation with time of the relative lateral (shear) motion Δx of the surfaces across the confined liquid. At large surface separations D, and with no motion applied to the top surface, Δx responds to external ambient

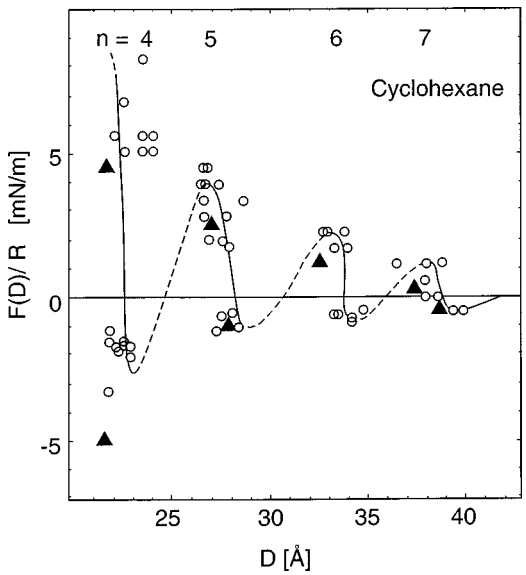

FIG. 3. Force (F)-distance (D) profile between curved mica surfaces (plotted as $F(D)/R$ where R is the mean radius of curvature) in a crossed cylinder configuration in cyclohexane. Solid triangles: data from Ref. 17. As in earlier investigations of structural forces Refs. 17, 21, and 46–48, the values of D are with respect to zero determined for dry air contact between the surfaces.

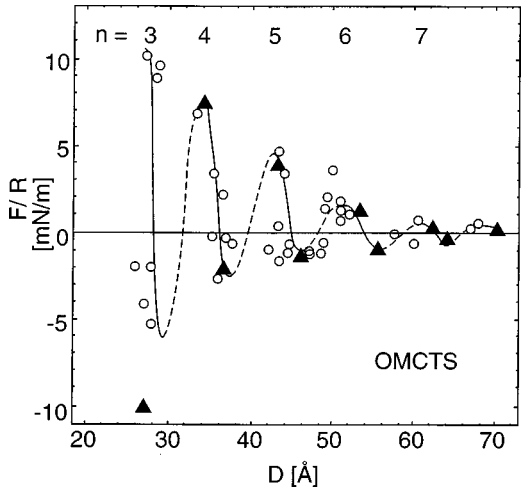

FIG. 4. $F(D)/R$ profiles in OMCTS. Solid triangles: data from Ref. 17.

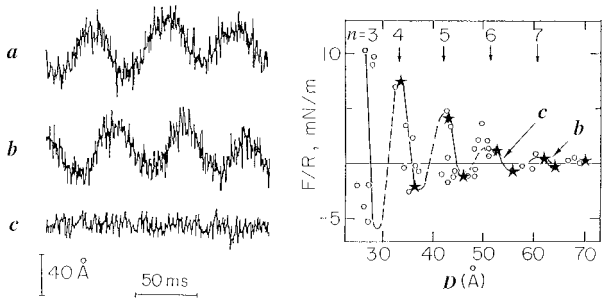

FIG. 6. Left-hand side: Direct recordings (from a recording oscilloscope) of the variation in time of the relative lateral displacement Δx of the mica surfaces immersed in OMCTS (with no applied lateral motion) at separations as follows: trace (a) $D=1160$ Å; trace (b) $D=62\pm2$ Å; trace (c) $D=54\pm2$ Å. Traces (b) and (c) correspond to points *b* and *c* on the force distance profile for this liquid reproduced (from Fig. 4) on the right-hand side.

noise at the characteristic frequency (ca. 17 Hz) of the spring S_1, as shown in trace 6(a) ($D=1160$ Å). When the surfaces are brought closer together, these random vibrations persist down to $D=62\pm2$ Å, trace 6(b); this corresponds to point *b* on the normalized force profile, as shown on the right of the traces, at $n=7$ molecular layers of OMCTS. Upon slight further compression, the surface separation decreased discontinuously to $D=54\pm2$ Å (point *c* on the normal force profile, corresponding to $n=6$). At this point, as seen in trace 6(c), the 17 Hz vibrations cease abruptly. This transition occurs over time scales shorter than we were able to measure (<0.5 s). The change in confinement from seven to six molecular layers has all at once rendered the film solid enough to resist the random lateral shearing motion induced by the external noise. The transition is reversible, that is, on increasing the separation to $D>6$ monolayers, random vibrations (at ca. 17 Hz) are observed again. Moreover, the transition to the solid-like (shear-stress sustaining) phase is induced by the additional confinement alone: little normal pressure on the OMCTS is necessary (see caption to Fig. 6). Once the $n=7\rightarrow n=6$ transition has taken place, the confined OMCTS retains its solidlike characteristics even if the applied small normal force [corresponding to point *c* on the right-hand side (RHS) of Fig. 6] is reduced to zero.

The sharp transition observed for OMCTS at the confinement change $n=7\rightarrow n=6$ is characteristic also of the other liquids studied, though it could take place at slightly different confinements. For cyclohexane the abrupt change manifested in Fig. 6 was generally observed as $n=7\rightarrow n=6$. However, in one or two instances where ambient noise was especially low (in late night experiments) the transition was seen for a change in layer spacing $n=8\rightarrow n=7$, and

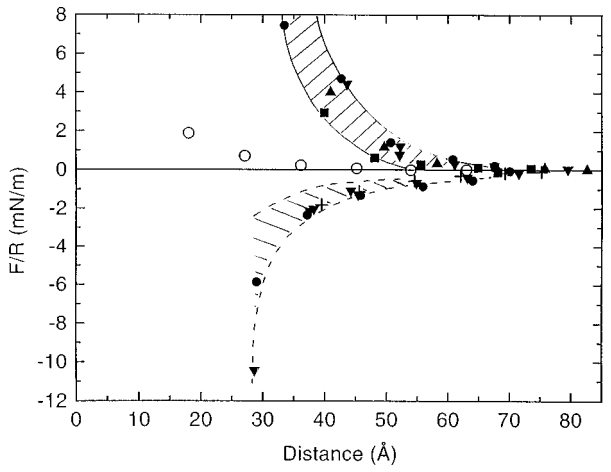

FIG. 5. Comparison of force-distance profiles in OMCTS from several independent studies (▼, Ref. 17; ▲, Ref. 46; ■, Ref. 47; +, Ref. 48) with the present data (●). The solid points are the maxima and minima of the $F(D)/R$ variation for samples that have been distilled or double-distilled. The shaded bands include scatter in all data. The open circles (○) are from a study (Ref. 21) where the OMCTS was used as received, under dry conditions but without distillation (no data for minima were reported in this study).

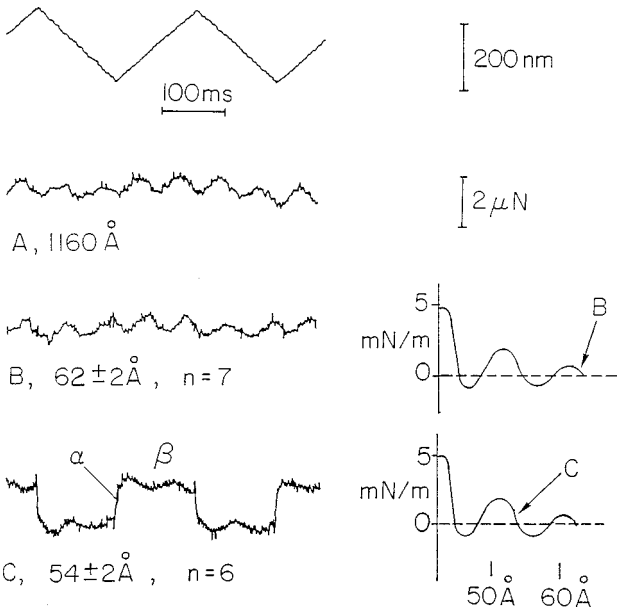

FIG. 7. Top trace: Lateral back-and-forth motion applied to the top mica surface when sliding past the lower surface across OMCTS. Traces A, B, and C correspond to the surface separations (or *n* values) shown; the normal forces for traces B and C correspond to the points *B* and *C* shown on the right-hand side force profiles for OMCTS reproduced from Fig. 4.

solidlike behavior in cyclohexane was manifested in these conditions already for $n=7$. For toluene, the abrupt liquid-to-solid change was observed at the $n=5\rightarrow n=4$ transition. We discuss the nature of these transitions in more detail later.

A more quantitative manifestation of this liquid-to-solid transition was obtained by applying a controlled lateral motion to the top mica surface via the piezoelectric tube and measuring directly the resulting shear force $F_s(D)$ between the surfaces. This is shown for the case of OMCTS in Fig. 7: as the top surface is moved laterally at a uniform velocity, first in one direction and then in the other, top zig-zag trace in Fig. 7, the shear force transmitted to the lower surface by the confined OMCTS is recorded directly in the traces shown. At surface separations from $D=1160$ Å down to $D=62\pm 2$ Å ($n=7$) no shear response is detected within the noise level of the signal, as seen from traces A ($D=1160$ Å) and B ($D=62$ Å) of Fig. 7 [trace B is taken at point B on the $F(D)/R$ plot to the right of the trace]. When the surfaces are moved together to $D=54\pm 2$ Å ($n=6$), the form of the shear stress transmitted by the OMCTS changes sharply [trace C of Fig. 7, taken at point C on the adjacent $F(D)/R$ plot]. The response is now characteristic of a solid confined between two surfaces: an initial elastic regime, as the shear stress rises to a yield point (region α in curve C), is followed by a ''plastic'' deformation of the OMCTS in the gap, as for a ductile solid under shear. The two confining surfaces then slide past each other at a uniform mean velocity (region β in curve C). This behavior is similar to that shown in Fig. 2, trace D, though the data averaging in trace C of Fig. 7 has obscured any stick-slip behavior.

1. Effective viscosity prior to the liquid-to-solid transition

The shear force data of Fig. 7, trace B show that the response $F_s(D)$ of OMCTS films only seven molecular layers thick is liquidlike and similar to that of much thicker films, as in trace A, and that both are within the signal resolution δF_s. Qualitatively similar behavior was observed for confined cyclohexane. We may use this observation to estimate from our data an upper limit on the viscosity corresponding to this response of the liquids confined between the mica surfaces. We focus on OMCTS, and consider the behavior in the liquidlike regime at film thickness corresponding to $n=7$ monolayers just prior to the transition.

The configuration of the crossed cylindrical mica surfaces near the region of closest approach is equivalent to that of a sphere, radius R (≈ 1 cm) a distance D from a plane. The force $F_s(D)$ required to move a sphere in a liquid medium of Newtonian viscosity η at constant velocity v_s parallel to a plane wall a distance D away, for $D\ll R$, is given by a series expansion whose leading term is[53]

$$F_s(D)=\left(\frac{16\pi}{5}\right)v_s\eta R\ \ln(R/D). \tag{1}$$

Thus for $D<100$ nm, the range of the present study, the force on the moving sphere is dominated by its viscous interactions with the wall. Equation (1) applies for the case where the viscosity η is constant. For the case where the viscosity may change with the confinement we need a different approach, since the extent of confinement (and thus the viscosity) changes across the gap due to the curvature of the surfaces. We need to extract from the shear force $F_s(D)$ between curved surfaces, a closest distance D apart across a liquid, the effective viscosity of a film of the same liquid confined between flat parallel plates a distance D apart. We require, in effect, the equivalent for the shear forces of the ''Derjaguin approximation'' for normal forces. This is done in Appendix A where it is shown that the effective mean viscosity of the liquid confined to a layer of thickness D is given by

$$\eta_{\text{eff}}\approx\frac{(\partial F_s(D)/\partial D)}{\left(\frac{16\pi}{5}\right)R\dot{\gamma}}, \tag{2}$$

where $\dot{\gamma}=(v_s/D)$ is the shear rate at the point of closest approach. In our experiments $F_s(D)$ is within the noise level $|\delta F_s(D)|\approx 0.5\ \mu$N throughout the range $\Delta D=(116-6.2\ \text{nm})$, as seen from curves A and B of Fig. 7. Approximating $\partial F_s(D)/\partial D$ by $(\delta F_s(D)/\Delta D)$ in this range,[54] we find that for $D=6.2$ nm (i.e., seven monolayers of OMCTS) and $v_s=1600$ nm/s (Fig. 6), this gives an upper estimate on η_{eff} of ca 3 P (poise).

2. Contact area between surfaces following the transition

The analysis above treated the material between the surfaces prior to the liquid–solid transition as fluid, and the solid confining surfaces themselves as remaining curved. Following the transition the confined material is solidlike: it can then sustain a shear stress, and a flattening of the two confining mica surfaces under normal load or due to attraction may occur in the presence of the confined film (see Fig. 13 in Appendix B). We require the area $\mathscr{A}$ of this flattened region between the surfaces as they are sheared at different loads and film thicknesses. In general, it is only at normal loads $F_n/R\geqslant 4$ mN/m that measurable flattening of the curved mica surfaces (and thus a measurable $\mathscr{A}$), is produced by distortion of the glue/mica layers. Most of the range of interest for the study of films of thickness corresponding to $n=3-7$, for both cyclohexane and OMCTS (see Figs. 3 and 4), is at lower loads. In this case $\mathscr{A}$ is evaluated using the Johnson–Kendall–Roberts (JKR) model[55] for contact between curved, adhering surfaces of finite compressibility. According to this, for a sphere in contact with a rigid flat (equivalent to the geometry of our crossed cylindrical surfaces), a circular contact area of radius a is formed at the contact position when the two are compressed by a force F_n, such that

$$a^3=\frac{R}{K}\left[F_n+2F_p+2(F_nF_p+F_p^2)^{1/2}\right]. \tag{3}$$

Here R is the radius of the undeformed sphere [$R=(R_1R_2)/(R_1+R_2)$ for contact between crossed cylinders of radii R_1, R_2]; K is related to the Youngs modulus E of the sphere, as $K=(2/3)(E/(1-\nu^2))$ where ν is the Poisson ratio of the material (the two contacting solids assumed to be of

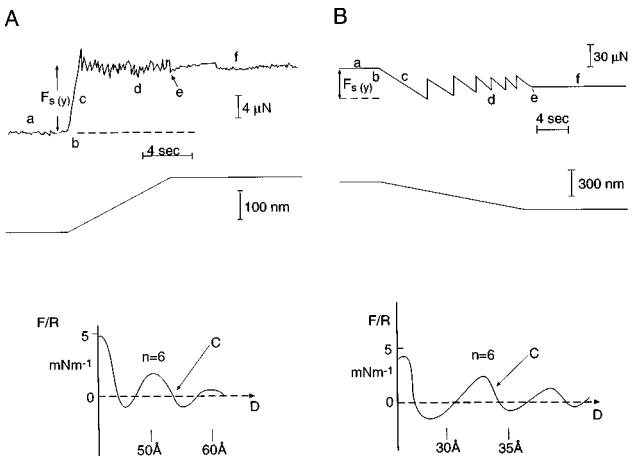

FIG. 8. (A) The top trace shows the shear force between two mica surfaces across an OMCTS film of thickness $n=6$ molecular layers, in response to the motion applied to the upper surface given by the second trace. Points $a-f$ refer to different stages in the shearing motion as noted in the text. The normal force between the surfaces is $F/R=0.14$ mN/m, corresponding to the point C on the OMCTS force-distance profile shown; the area of contact $\mathscr{A}$ for this load for OMCTS for $n=6$, evaluated from Eq. (3), is $\mathscr{A}=(1.2\pm0.3)\cdot10^{-10}$ m^2. (B) As for (A) but with a film of $n=6$ molecular layers of cyclohexane. The normal force between the surfaces is $F/R=1.67$ mN/m, corresponding to the point C on the cyclohexane force-distance profile shown; the area of contact $\mathscr{A}$ for this load for cyclohexane at $n=6$, evaluated from Eq. (3), is $\mathscr{A}=(1.9\pm0.3)\cdot10^{-10}$ m^2.

the same material); and F_p is the pull-off force required to separate the two surfaces against the adhesion force between them. The contact area is then given by $\mathscr{A}=\pi a^2$. In our experiments, the radii R_1 and R_2 are measured in the standard way from the shape of the interference fringes near the point of closest approach of the (separated) surfaces. The force F_p corresponds directly to the depth of the attractive well in the $F(D)$ profile that is associated with the number of molecular monolayers in the film being studied. The modulus K in our experiments refers to the three-layer composite glass-glue-mica. It was estimated by measuring the actual area of contact between the surfaces under normal forces large enough to produce a measureable flattening of the surfaces: a value $K=(1\pm0.3)\ 10^9$ N/m^2 was evaluated. This value is comparable with that determined for the glass-glue-mica combination employed in earlier experiments,[56] where a different glue (EPON 1004) was used in a similar configuration of the surfaces.

3. Relaxation under shear stress following the liquid-to-solid transition

Figure 6 and 7 demonstrate that the changes in mechanical properties of the confined phases following the liquid–solid transition at $n=7\rightarrow n=6$ are striking. A measure of the rigidity of the solidlike phases following the transition may be obtained from their resistance to creep under stress, a process which may be quantified in terms of an effective ''creep viscosity'' $\eta_{\rm eff}$. While it is not in general appropriate to characterize solidlike materials by a viscosity, a measure of such a viscosity is nonetheless instructive for highlighting the changes that take place at this transition. An estimate of $\eta_{\rm eff}$ was obtained by monitoring the relaxation of the film in its solidlike phase following an applied shear stress, as illustrated in Fig. 8(A) and 8(B) for OMCTS and cyclohexane, respectively.

In both cases (OMCTS and cyclohexane) shown in Fig. 8 the films are six monolayers thick, having just gone through the liquid-to-solid transition. They are at points indicated by C on the respective normal force profiles shown in the lower parts of Figs. 8(A) and 8(B) for the two materials. The mica surfaces interact via a contact area $\mathscr{A}$ (different for the two cases), evaluated from the JKR model as described above. The configuration in each case [Figs. 8(A) and 8(B)] is then one of a Couette-like geometry where a film of area $\mathscr{A}$ and thickness D is subjected to a shear force F_s applied via a spring of constant K_1 [see Fig. 13 in Appendix B]. Initially, the film confined between the two surfaces is under zero shear force, $F_s=0$ [region a in Figs. 8(A) and 8(B)]; at points b a steady lateral motion at velocity $v_s=(dx/dt)$ is applied to the top surface. At first the shear force across the film rises (region c) to a yield value $F_{s(y)}$. Subsequently, the surfaces slide past each other, via a stick-slip motion, with a mean velocity v_s. In this regime [region d in Figs. 8(A) and 8(B)] the shear force across the film oscillates due to the stick-slip motion, but its mean value remains essentially constant at $F_s\leqslant F_{s(y)}$. The applied motion is then stopped [points e], and the relaxation of the shear force due to creep of the confined phase [regions f in Fig. 8] is monitored by observing the change in F_s. For both materials, OMCTS, Fig. 8(A), and cyclohexane, Fig. 8(B), the extent of relaxation in F_s over the times shown is very low: it is within the noise level of the signals in the two cases. In Appendix B the relaxation of the shear force F_s due to creep of the confined film in this Couette geometry is considered: for a decay ΔF_s ($\ll F_{s(y)}$) in F_s over a time Δt, the effective creep viscosity is given by

$$\eta_{\rm eff}=\frac{F_{s(y)}K_1D\Delta t}{\Delta F_s\mathscr{A}}. \tag{4}$$

Focusing again on OMCTS we have, for the trace of Fig. 8(A), $F_{s(y)}=9.5\ \mu$N and $\mathscr{A}=(1.2\pm0.3)\times10^{-10}$ m^2; over a period $\Delta t=10$ s the decay is within the noise level, $\Delta F_s<\delta F_s=0.3\ \mu$N. This gives from Eq. (4) a lower limit on the effective creep viscosity, $\eta_{\rm eff}\geqslant6.10^7$ P.

C. Variation of shear stress with shear velocity

The variation with shear rate of the shear stress in confined films just subsequent to the liquid–solid transition, and under essentially zero applied pressure, is of particular interest. This is because the variation of shear stress with sliding velocity is qualitatively very different in liquids and solids. The shear response of such films as a function of the mean relative shear velocity (or, equivalently, shear rate) of the surfaces is shown in Fig. 9. The data shown is for OMCTS films with $n=6$ monolayers ($D=63\pm2$ Å). Figures 9(a)–9(c), top traces, show the back-and-forth applied motion of the top mica surface at a number of different velocities v_s, together with the corresponding shear forces, lower traces. v_s could be conveniently varied by changing the rate at which the potential was applied to the PZT. We observe at once

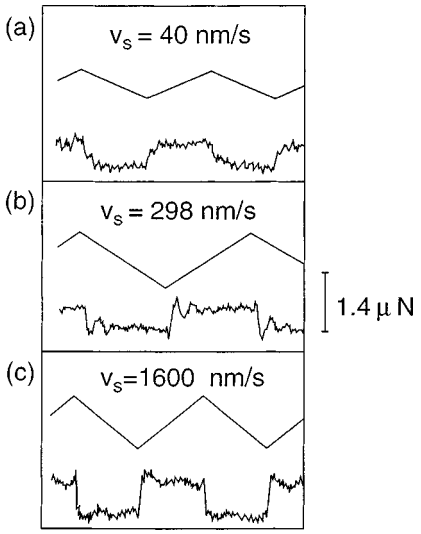

FIG. 9. The top trace in each of (a)–(c) shows the back-and-forth motion applied to the upper mica surface sliding relative to the lower mica surface across a film of $n=6$ monolayers of OMCTS ($D=52\pm3$ Å); the lower trace in each of (a)–(c) shows the corresponding shear forces between them. v_s are the applied velocities. The scale bar in the force applies to all three cases. The normal loads are (a) $F/R=0.01\pm0.1$ mN/m; (b) $F/R=-0.06\pm0.1$ mN/m; (c) $F/R=-0.09\pm0.1$ mN/m.

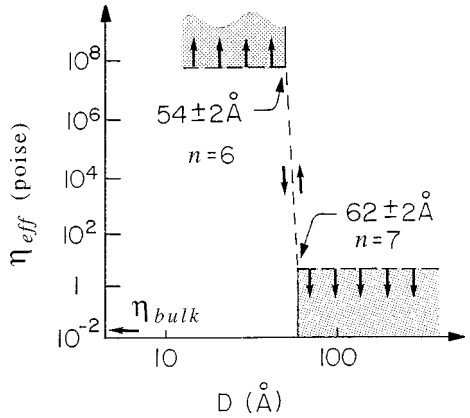

FIG. 10. Variation with film thickness D of the effective mean viscosity $\eta_{\rm eff}$ of confined OMCTS films (on a double-logarithmic plot) determined as described in text. The broken lines at $D<54$ Å and at $D>62$ Å are lower and upper limits on $\eta_{\rm eff}$, respectively. The bulk viscosity of OMCTS at 23 °C is indicated as $\eta_{\rm bulk}$. The reversibility indicated at $D=62\leftrightarrow54$ Å refers to the transition in the dynamical properties of the confined OMCTS.

that although v_s varies over a factor of 40, there is little change in the shear response between the traces. We note that for all three cases shown the applied normal load is extremely small (<1 μN), so that the solidlike behavior observed is induced effectively by confinement alone. The clear conclusion from these traces (which are typical of others) is that the shear stress is independent (or only very weakly dependent) on the shear velocity. This is true for both cyclohexane and OMCTS (the variation of F_s with v_s for toluene was not investigated) just following the liquid-to-solid transition. This behavior is characteristic of a solid, since for a liquid one expects the shear stress to be proportional to the shear rate. In the following paper (II), we describe how thinner films well in the solidlike regime ($n=5-3$), respond to shear at much higher pressures and over a wider range of v_s. We find, in agreement with Fig. 9, that the mean stress to slide the surfaces past each other remains largely independent of the sliding velocity for all these layer thicknesses, particularly at the highest shear rates used.

IV. DISCUSSION

Two particular features of the surface force balance used in the present study, true parallel motion (to ±1 Å over a range of lateral motion of order 1000 Å) and extreme sensitivity in measuring shear forces directly, allow us to probe in detail the dynamic properties of thin films between solid surfaces. In particular, these features enable the determination of shear forces between the surfaces across confined simple liquids even in the absence of any applied compressive (normal) forces. This permits us to examine in detail the change in properties of the progressively confined layers from the liquid to the solidlike states. This was not possible in the earlier pioneering shear studies of simple liquids confined between curved surfaces.[5,6,15] (We recall that the present apparatus is capable of a sensitivity and resolution in measuring shear forces some three orders of magnitude higher than in the earlier studies.) In these, large compressions had to be applied to flatten the surfaces at the region of contact, so that the overall shear forces became large enough to measure. These large compressions squeezed the liquids being probed to films some three or fewer monolayers thick, well within the solidlike regime. In our study we were able to investigate in detail much thicker films, and so to access the confinement-induced liquid-to-solid transition.

Our main new finding is the sharp transition on increasing confinement between films of thickness corresponding to $n=(n_c+1)$ monolayers, where the confined material was liquidlike, and films just one monolayer thinner, $n=n_c$, where the confined films were able to sustain a shear stress over macroscopic times. This ability to sustain a shear stress is a fundamental signature of a solid: a liquid, by definition, cannot sustain such a stress. The critical thickness n_c measured in our experiments varied somewhat between the different liquids: $n_c=6$ for OMCTS, $n_c=6$ or 7 for cyclohexane, and $n_c=4$ for toluene. A convenient way of quantifying this transition is via the change in $\eta_{\rm eff}$ across the transition (Secs. III B 1 and III B 2). This is shown in Fig. 10 for OMCTS, where an increase of at least 7 ± 1 orders of magnitude in the effective viscosity is observed as the confinement goes from $n=n_c+1$ ($=7$) layers of the liquid, at $D=62\pm2$ Å, to $n=n_c$ ($=6$) layers. The limits are set by the signal-to-noise ratio of our measurements, as described in Sec. III. Similar effects were observed also for cyclohexane and (qualitatively) for toluene, at the respective n_c values. Within the range of our parameters, there is clearly no evidence whatever of an ''intermediate'' regime of progressively increasing viscosity on increasing confinement for these liquids, as reported earlier for a number of liquids,[19–21] including OMCTS. The origins of this discrepancy in the case of OMCTS may be related to different procedures in sample processing.[57]

The abruptness and magnitude of the change at the confinement-induced transition seen in Fig. 10 are reminis-

cent of a first-order transition, and suggest that at the transition the entire film locks into a solid structure. We note also that this transition is brought about by increasing confinement alone, with little applied external pressure (see, e.g., data of Fig. 9). Finally, we remark that this effect is seen for liquids (cyclohexane, OMCTS, and toluene) whose molecular size (Table I) differs appreciably from each other as well as from the crystal periodicity of the confining mica surfaces; this indicates that epitaxiality with the surface lattice is not necessary for inducing the transition in such simple liquids. It would be extremely interesting, and challenging, to be able to probe the in-plane and normal-to-plane structural features of the confined solid on both sides of the transition. However, the geometry of the confinement and the extremely small volume of interest within the gap render this well beyond the present capabilities of x-ray techniques.[58]

Insight into the origin of this transition may be obtained from the following considerations. Both experiments and computer simulations[8–10,59] suggest that simple bulk liquids in contact with a single planar surface undergo some layering, extending to a few molecular diameters away from the surface. This layering is due to geometric packing, and is similar to, but more marked and longer ranged than the density oscillations about a single liquid molecule revealed by its radial distribution function (it may be viewed as corresponding to the radial distribution function of the liquid molecules about a ''molecule'' of radius R, where $R\rightarrow\infty$). Despite this layering, as noted in the Introduction, experiments have revealed[11–13] that unconfined liquids [or liquids confined to large gaps ($n\gg 10$)] retain their fluidity, with viscosities comparable to bulk viscosity, right up to the liquid/confining-solid interface (to within a single molecular layer). Layering, in other words, does not necessarily result in solidity. This at once implies that we are not dealing with several immobilized molecular layers on each mica surface, when they are far apart, that merely shift the effective solid–liquid interface away from the surface. Rather, the picture that emerges is that, as the surfaces approach each other from large separations, the confined liquids retain their bulk fluidity across the entire gap, until at a critical spacing the entire film undergoes a liquid-to-solid transition.

This transition appears to be due to a synergistic effect, produced by the confinement, and reminiscent, we suggest, of a Lindemann-like criterion:[60] At gap spacings greater than the critical value n_c, the layered molecules are less ordered and have a freedom of displacement greater than some necessary fraction of their mean spacing. At gaps n_c or thinner, the confinement suppresses this freedom to move to below the necessary fraction, and the entire confined liquid ''freezes.'' Alternatively we may think of the layering about each isolated surface as leading to a slightly higher mean density in the near-surface region. When the surfaces approach, these near-surface regions overlap each other. This results in an overall mean density within the intersurface gap that leads to the Lindemann crossover. Thermodynamically, this effect may be viewed in terms of the associated entropic changes. For $n>n_c$ the entropy associated with local liquidlike translational motion of the confined molecules results in a greater free-energy reduction than the enthalpic gain resulting from fixing them in a solidlike lattice. For $n\leqslant n_c$, the smaller space available to the confined molecules reverses this, and a solidlike behavior results. This picture is illustrated schematically in Fig. 11. This effect should depend in a sensitive fashion on the excess temperature of the measurements above the bulk melting temperature of the liquid, as well as on the detailed surface–liquid interactions.

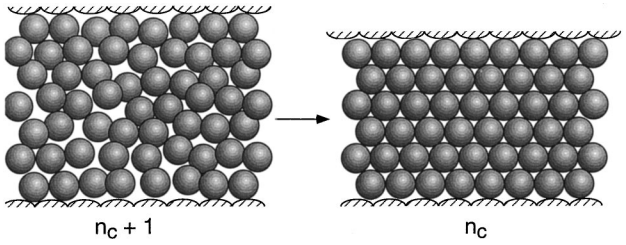

FIG. 11. Illustrating schematically the transition between a layered but fluid film of thickness n_c+1 molecular layers, and one of thickness n_c with a layered but frozen structure.

The above discussion is clearly rather qualitative. There have been several detailed theoretical and computer simulation studies of the effects, both on structural and mechanical/dynamic properties, induced by confinement on liquids of both spherical and linear molecules.[22,23,25–29,33,59,61–63] These have shed much light on the processes that may be taking place as liquids are confined to progressively thinner films, and as the films are sheared. The details of the models do not exactly tally with the conditions of our experiments (for example, the liquid molecules are often assumed to be identical to the surface molecules, and are taken as perfect hard spheres), precluding detailed comparisons, but there have been several very suggestive findings. Here we focus briefly on those studies that provide clues to the issue of the liquid-to-solid transition under increasing confinement.

As noted, the geometric constraints of smooth walls lead to layering of spherical molecules,[8,9] even in the vicinity of a single unconfined surface, though this is not necessarily correlated with freezing.[62] In-plane ordering[22] (in addition to the layering) and correlated freezing[23] were observed by Cushman, Schoen, Diestler and Rhykerd in simulations of rare-gas fluids confined between two solid surfaces. In related theoretical work[24] these authors have also shown that, under sufficient confinement, liquids can form epitaxially growing solids with a thermodynamically stable configuration. A convenient measure of in-plane order is the Debye–Waller factor (DWF), defined in terms of the two-dimensional structure factor within a layer, whose value is unity in a perfect crystal at zero temperature, and drops to 0.6 at the melting point.[64] Molecular dynamics simulations by Robbins, Thompson, and Grest[26,65,66] indicate that for confined spherical molecules the DWF rises sharply on increasing confinement from a value below 0.6 (i.e., liquidlike) to one above it (solidlike) when the confined liquid is compressed to below a given thickness. In contrast, for chainlike (nonspherical) molecules the DWF remained lower than 0.6 (indicating a more liquidlike in-plane order) at all accessible compressions in their study.

Another useful measure of solidity of confined liquids is

the self-diffusion coefficient D_s within the layers, which is related to the effective viscosity. In simulations[10,26,33,65] this has been shown to drop abruptly when films (of spherical molecules) are confined below a given film thickness (correlated to the point where the DWF exceeds 0.6), again indicating a rather sharp solidification process.

Some of the most suggestive indications concerning confinement-induced liquid-to-solid transition in thin films have come from very recent simulation work by Landmann and co-workers,[27,33] who use a grand canonical ensemble molecular dynamics method to simulate confined liquids. Their results show clearly that molecules that are able to pack easily (unbranched linear alkanes and also spherical molecules resembling OMCTS) undergo a rather sudden change in their properties (a very sharp drop in the diffusion coefficient, for example), from liquidlike to solidlike behavior, at film thicknesses corresponding to around five to six layers. Moreover, at this point the confined films in their studies become capable of sustaining a shear stress. These observations suggest an abrupt liquid-to-solid transition at these confinements, very similar to the experimental observations of the present study.[7] This contrasts with the simulated behavior of branched or irregularly shaped molecules (such as squalane) which exhibit a monotonic and continuous (liquidlike) decrease in the number of confined molecules as the film thickness decreases.[27,33] The models of these studies are necessarily cruder than reality even with liquids such as OMCTS and cyclohexane which have quasi-spherical molecules. Their results, however, are fully consistent with our observation of an abrupt liquid–solid transition at a given film thickness for these simple liquids.

Recently the issue of confinement induced freezing has been examined explicitly using different analytical approaches. Tkachenko and Rabin[31] have presented a model based on a Lindemann criterion to show that at a given layer spacing, a confined liquid would solidify abruptly even above its bulk melting temperature. Weinstein and Safran[32] have used a density functional approach, with the additional constraint of the two confining surfaces, to determine a phase diagram for the confined liquid, and again a confinement-induced freezing is predicted to occur abruptly at temperatures where the bulk material would be liquid. Both of these approaches have the advantage that in principle they can predict the effect of temperature on the necessary confinement at which the freezing occurs, and for both models the freezing is predicted to occur as a result of confinement alone: i.e, in the absence of external pressure. This is in line with the observations of the present study.

We make a final brief remark concerning the variation of shear stress with shear rate indicated in Fig. 9. This shows how the shear stress between sliding mica surfaces across an $n=6$ film of OMCTS (film thickness $D=53\pm2$ Å), that is, just after the liquid–solid transition, varies with sliding velocity. The velocities v_s vary by a factor of 40, corresponding to shear rates $\dot{\gamma}=(v_s/D)$ in the range $8-300\ \mathrm{s}^{-1}$, while the applied normal pressures P are close to zero (see caption). Within the scatter, the shear stress S_c is essentially identical for all three shear velocities (the small differences are well within the uncertainty in shear stress expected from the uncertainty in the normal load). This independence of the shear stress from the shear rate[67] (i.e., $S_c \propto \dot{\gamma}^0$) is clearly characteristic of shearing of a ductile solid,[68] rather than of a liquid or a liquidlike film. We return to this point in the following paper (II) when we consider a much broader range of data on liquids confined to even thinner films ($n=3-6$).

V. SUMMARY

We have described a surface force balance with extremely high sensitivity and resolution in measuring shear forces across thin films. Using this we have extended earlier investigations on the properties of confined simple liquids to thicker films and lower applied pressures. Here we have focus on the process by which simple liquids become solid under increasing confinement.

We discovered that the transition between liquidlike behavior and a solidlike phase of the liquids under progressive confinement takes place abruptly at a well-defined film thickness (equivalent to n_c monolayers of the liquid, where n_c varied with the liquid but was around six molecular layers). For thinner films ($n \leqslant n_c$) the films behaved in a solidlike fashion, in the sense of requiring a critical stress in order to shear them. We found no evidence of an intermediate regime of increasingly viscous behavior for the three simple liquids studied. Our results are reminiscent of a Lindemann-like mechanism for freezing of a liquid, save that the changes are induced by confinement, rather than by externally applied pressure or by changes in temperature. In the following paper[69] (II) we describe in detail the mechanical, frictional, and dynamic behavior of such confined films once they had solidified.

ACKNOWLEDGMENTS

We thank R. Ball, H. Christensen, S. Granick, G. Grest, J. Israelachvili, M. Robbins, U. Landmann, Y. Rabin, S. Safran, and A. Weinstein for useful comments and correspondence, and U. Landman for providing us with a copy of Ref. 33 prior to publication. This work was supported by the Israel Science Foundation, the Ministry of Science and Arts (Israel-Tashtit programme) and the U.S.-Israel Binational Science Foundation.

APPENDIX A: A "DERJAGUIN APPROXIMATION" FOR SHEAR FORCES BETWEEN CURVED SURFACES

The Derjaguin approximation[70] for normal forces between two curved surfaces a closest distance D apart relates the normal force $F(D)$ between them to the interaction energy per unit area between flat parallel plates a distance D apart obeying the same force-distance law, as

$$F(D)/2\pi R = E(D) \quad (R \gg D), \tag{A1}$$

where R is the mean radius of curvature of the surfaces. When two curved surfaces a closest distance D apart are moving with velocity v_s parallel to each other across a medium with some effective viscosity η_{eff} (which may be a function of D), a shear force $F_s(D,v_s)$ will result. In this Appendix we derive[71] an approximate expression for the

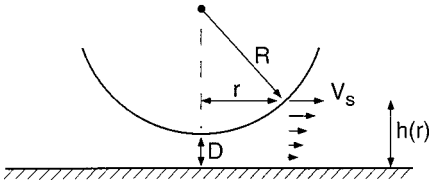

FIG. 12. Illustrating the geometry of a sphere sliding at velocity v_s a closest distance D from a plane as discussed in Appendix A.

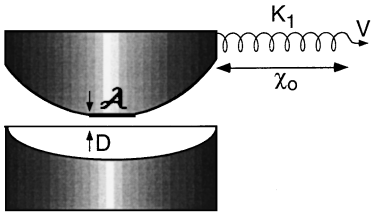

FIG. 13. Illustrating the stress relaxation in a couette geometry when the upper surface is under tension due to spring S_1 and is in contact over a film of area $\mathscr{A}$ and thickness D with the lower surface, as for the data of Fig. 8 and as discussed in Appendix B.

equivalent shear stress $S(D,v_s)$ between flat plates sliding parallel to each other at velocity v_s a distance D apart across a medium obeying the same viscosity versus thickness law (i.e., the same variation of η_{eff} with D). This is particularly useful since theoretical models of shear forces often treat flat parallel plates rather than curved surfaces. To be explicit, we treat the case of a sphere, radius R, sliding parallel to a plane a closest distance D away (in the lubrication limit $R \gg D$).

It is instructive to derive first, via a crude model, the shear force between a sphere moving at velocity v_s in a fluid of uniform (Newtonian) viscosity η parallel to a plane a distance D away, as illustrated in Fig. 12. The main simplification of this model is the assumption of laminar flow, i.e., no backflow effects. We consider the forces on an annulus of radius r as shown. From the geometry, $r^2=2R(h-D)$, i.e.,

$$h(r)=D+(r^2/2R)\,. \tag{A2}$$

The shear rate at r is $(v_s/h(r))$, so that the local Newtonian shear stress $\sigma(r)=\eta(v_s/h(r))$. Integrating stresses over the annuli for the total shear force,

$$\begin{aligned} F_s &= \int_0^R 2\pi r\sigma(r)dr \\ &= \int_0^R 2\pi r\eta\,\frac{v_s}{D+(r^2/2R)}\,dr \\ &= 2\pi\eta v_s R\,\log(1+(R/2D)) \\ &\approx 2\pi\eta v_s R\,\log(R/D) \end{aligned} \tag{A3}$$

since in the geometry of our experiments $R/D=10^5$. Now a detailed solution of the force acting on a sphere sliding close to a plane has been carried out by Goldman *et al.*[53] These authors show, using the Navier–Stoke equations and thus taking the correct flow field into account, that the force is given by a series expansion whose dominant term (for $R \gg D$) is

$$F_s(D)=(16\pi/5)v_s\eta R\,\ln(R/D). \tag{A4}$$

Comparison of (A3) and (A4) shows that the value of F_s derived in a calculation which ignores the backflow effects on the flow field has precisely the right form (in particular the correct logarithmic dependence), and differs in magnitude from a detailed calculation only by some 35%. This observation will be useful in what follows.

To extract $S(D,v_s)$ in the more general case where the effective viscosity in the gap may vary with D, we proceed as follows. From the geometry of Fig. 12, we have $h=D+(r^2/R)$. Thus $dh=(r/R)dr$, and the area dA of an annulus may be written as $dA(h)=2\pi r dr=2\pi R dh$. The overall force between the surfaces is then as before (ignoring any backflow effects) the sum of the forces over all annuli, given by

$$F_s(D,v_s)=\int_D^\infty S(h,v_s)dA(h)=\int_D^\infty 2\pi RS(h,v_s)dh, \tag{A5}$$

where we have put the upper integration limit as ∞ since $R \gg D$.

From (A5) we have

$$S(D,v_s)=-\frac{1}{2\pi R}\,\frac{\partial F_s(D,v_s)}{\partial D}. \tag{A6}$$

This is the relation we have been seeking, giving the shear stress $S(D,v_s)$ between flat parallel plates in terms of the shear force $F_s(D,v_s)$ between curved surfaces. Finally we recall that neglect of backflow effects leads to some error, which for the simple Newtonian case was equivalent to replacing the prefactor 2π by $(16\pi/5)$, a change only in the numerical prefactor by some 35%, as discussed following Eq. (A4) above [compare Eqs. (A3) and (A4)]. If, by extrapolation, we make the rough assumption that the inclusion of backflow has the same effect also in the case where the viscosity is confinement dependent, we may make the same correction to Eq. (A6), to give finally

$$S(D,v_s)\approx-\frac{1}{(16\pi/5)R}\,\frac{\partial F_s(D,v_s)}{\partial D}. \tag{A7}$$

Replacing the shear stress in (A7) by the Newtonian form $S(D,v_s)=\eta_{\text{eff}}\dot{\gamma}$, where $\dot{\gamma}=(v_s/D)$, leads at once to Eq. (2) in the text.

We note that care should be taken when extracting $S(D,v_s)$ from shear measurements between curved surfaces. In particular, $S(D,v_s)$ is obtained from data on $F_s(D,v_s)$ taken over a range of D at fixed shear velocity v_s.

APPENDIX B: STRESS RELAXATION IN A COUETTE CONFIGURATION

The geometry of the contacting surfaces when the top one is pulled by a spring (corresponding to the shear spring S_1 in Fig. 1, of constant K_1) is shown in Fig. 13. The area of contact is $\mathscr{A}$, enclosing a film of thickness D with an effective viscosity η_{eff}, in steady motion the spring is stretched to length x_0, and the steady-state velocity is v_s. During steady motion the tension K_1x_0 in the spring is balanced by the shear force $F_s(y)$ across the film:

$$K_1 x_0 = F_{s(y)} = \mathscr{A}.(\text{shear stress}) = \mathscr{A}\eta_{\text{eff}} v_s / D. \quad \text{(B1)}$$

At time $t=0$ the motion of the spring tip is stopped [corresponding to the point e in Fig. 8(A), for example]. At subsequent time t the top surface will have moved by a distance x, relaxing some of the force in the spring. The new balance of forces is

$$K_1(x_0 - x) = F_s(t) = (\mathscr{A}\eta_{\text{eff}}/D)(dx/dt), \quad \text{(B2)}$$

which is readily solved [subject to the condition (B1) at $t=0$] to give

$$F_s(t) = (\mathscr{A}\eta_{\text{eff}} v_s / D) e^{-t/\tau} = F_{s(y)} e^{-t/\tau}, \quad \text{(B3)}$$

where $\tau = (\mathscr{A}\eta_{\text{eff}}/K_1 D)$. The extent of relaxation after a time Δt is $\Delta F_s = F_{s(y)} - F_s(t)$, i.e.,

$$\Delta F_s = F_{s(y)}(1 - e^{-\Delta t/\tau}) = (\Delta t/\tau) F_{s(y)} \quad \text{(B4)}$$

for $\Delta Fs \ll F_{s(y)}$. Rearranging (B4) and substituting for τ gives Eq. (4) in the text.

[1] D. Tabor, *Friction* (Doubleday, New York, 1973).
[2] J. S. Rowlinson and B. Widom, *Molecular Theory of Capillarity* (Clarendon Press, Oxford, 1982).
[3] F. P. Bowden and D. Tabor, *The Friction and Lubrication of Solids* (Clarendon Press, Oxford, 1964).
[4] *Fundamentals of Friction*, edited by I. L. Singer and H. M. Pollock (Kluwer Academic, The Netherlands, 1992).
[5] J. Israelachvili, P. M. McGuiggan, and A. M. Homola, Science **240**, 189 (1988).
[6] J. Van Alsten and S. Granick, Phys. Rev. Lett. **61**, 2570 (1988).
[7] J. Klein and E. Kumacheva, Science **269**, 816 (1995).
[8] S. Toxvaerd, J. Chem. Phys. **74**, 1998 (1981).
[9] J. Magda, M. Tirrell, and H. T. Davis, J. Chem. Phys. **83**, 1888 (1985).
[10] M. Schoen, J. H. Cushman, D. Diestler, and C. Rhykerd, J. Chem. Phys. **88**, 1394 (1988).
[11] D. Y. C. Chan and R. G. Horn, J. Chem. Phys. **83**, 5311 (1985).
[12] J. N. Israelachvili, Colloid Polym. Sci. **264**, 1060 (1986).
[13] R. G. Horn, D. T. Smith, and W. Haller, Chem. Phys. Lett. **162**, 404 (1989).
[14] J. Klein, Y. Kamiyama, H. Yoshizawa, J. N. Israelachvili, G. Fredrickson, P. Pincus, and L. J. Fetters, Macromolecules **26**, 5552 (1993).
[15] M. L. Gee, P. M. McGuiggan, J. N. Israelachvili, and A. M. Homola, J. Chem. Phys. **93**, 1895 (1990).
[16] H. Yoshizawa and J. N. Israelachvili, J. Phys. Chem. **97**, 11300 (1993).
[17] H. K. Christenson, J. Chem. Phys. **78**, 6906 (1983).
[18] R. G. Horn and J. N. Israelachvili, J. Chem. Phys. **75**, 1400 (1981).
[19] S. Granick, Science **253**, 1374 (1991).
[20] H.-W. Hu, G. A. Carson, and S. Granick, Phys. Rev. Lett. **66**, 2758 (1991).
[21] A. L. Demirel and S. Granick, Phys. Rev. Lett. **77**, 2261 (1996).
[22] M. Schoen, D. J. Diestler, and J. H. Cushman, J. Chem. Phys. **87**, 5464 (1987).
[23] C. L. Rhykerd, M. Schoen, D. J. Diestler, and J. H. Cushman, Nature (London) **330**, 461 (1987).
[24] D. J. Diestler, M. Schoen, and J. H. Cushman, Science **262**, 545 (1993).
[25] P. A. Thompson and M. O. Robbins, Science **250**, 792 (1990).
[26] P. A. Thompson, G. S. Grest, and M. O. Robbins, Phys. Rev. Lett. **68**, 3448 (1992).
[27] J. Gao, W. D. Luedtke, and U. Landman, J. Chem. Phys. **106**, 5751 (1997).
[28] I. Hersht and Y. Rabin, J. Non-Cryst. Solids **172-174**, 857 (1994).
[29] M. Urbakh, L. Daikhin, and J. Klafter, Europhys. Lett. **32**, 125 (1995).
[30] M. G. Rozman, M. Urbakh, and J. Klafter, Phys. Rev. Lett. **77**, 683 (1996).
[31] A. Tkatchenko and Y. Rabin, Solid State Commun. **103**, 361 (1997); Langmuir **13**, 7146 (1997).
[32] A. Weinstein and S. Safran A, Europhys. Lett. (in press).
[33] J. Gao, W. D. Luedtke, and U. Landman, Phys. Rev. Lett. **79**, 705 (1997).
[34] A. I. Bailey and J. S. Courtney-Pratt, Proc. R. Soc. London, Ser. A **227**, 500 (1954).
[35] D. Tabor and R. Winterton, Proc. R. Soc. London, Ser. A **312**, 435 (1969); J. Israelachvili and D. Tabor, *ibid.* **331**, 19 (1972).
[36] J. N. Israelachvili and G. A. Adams, J. Chem. Soc. Faraday I **74**, 974 (1978).
[37] A. I. Bailey, J. Appl. Phys. **32**, 1407 (1961).
[38] J. N. Israelachvili and D. Tabor, Wear **24**, 386 (1973).
[39] B. J. Briscoe and D. C. B. Evans, Proc. R. Soc. London, Ser. A **380**, 389 (1982).
[40] J. Klein, D. Perahia, and S. Warburg, Nature (London) **352**, 143 (1991).
[41] J. Klein, E. Kumacheva, D. Mahalu, D. Perahia, and L. J. Fetters, Nature (London) **370**, 634 (1994).
[42] J. Klein, Annu. Rev. Mater. Sci. **26**, 581 (1996).
[43] J. Klein, Nature (London) **288**, 248 (1980).
[44] While shear motion can be applied to frequencies up to ν_m, shear forces can only be measured at frequencies $\omega < \omega_c \approx 17$ Hz, the resonance frequency of the springs K_1 when carrying the top lens mounting assembly.
[45] J. Janik, R. Tadmor, and J. Klein, Langmuir **13**, 4466 (1997).
[46] H. K. Christenson, Chem. Phys. Lett. **118**, 455 (1985).
[47] H. K. Christenson and C. E. Blom, J. Chem. Phys. **86**, 419 (1987).
[48] T. K. Vanderlick, L. E. Scriven, and H. T. Davis, Colloids Surf. **52**, 9 (1991).
[49] The data exclude the early pioneering report by Horn and Israelachvili (Ref. 18), where the presence of trace amounts of water was later implicated (Ref. 17) as being responsible for the weakness of the oscillations.
[50] Such impurities can come from the reactants diethoxydimethylsilane or (more probably) hexamethyldisiloxane. An additional possible side product is octamethyltrisiloxane. These have a linear structure, and if not removed they may suppress layering and mask the sharp liquid-to-solid transitions.
[51] H. K. Christenson, J. Phys. Chem. **90**, 4 (1986).
[52] Indeed, in a number of the early experiments where our distillation procedure was not adequate, with OMCTS in particular, oscillating surface forces were absent or much reduced. Similar suppression of the oscillating forces was observed also after several days of an experiment, by which time impurities, i.e., foreign molecules, had crept in [similar effects were seen by A. Berman and J. N. Israelachvili (private communication)]. In these cases we also did not observe the sharp liquid-to-solid transition on increasing confinement described in this paper. As noted, such experiments were aborted.
[53] A. J. Goldman, R. G. Cox, and H. Brenner, Chem. Eng. Sci. **22**, 637 (1967). We may use Eq. (2) for data as in Fig. 7 down to $n=7$ monolayers. This is because the normal forces between the surfaces are close to zero (point B in Fig. 7), while the adhesion due to oscillating forces is suppressed as long as the surfaces are sliding past each other, as shown in paper II (following). Thus the sliding surfaces retain their curvature with essentially no distortion [both F_p and F_n in Eq. (3) are zero or close to zero] and Eq. (2) remains valid.
[54] This is an approximation, since the change in the shear force δF_s may take place over a smaller range of ΔD. The effect of this approximation may be to increase the upper limit of η_{eff} just prior to the transition by as much as a factor of 10. We note also that the value we have taken for δF_s is itself also an upper limit and is probably much smaller: this acts to reduce the upper limit of η_{eff}. Overall, therefore, the upper limit of η_{eff} evaluated may have an uncertainty of about a factor of 10 in either direction.
[55] K. L. Johnson, K. Kendall, and A. D. Roberts, Proc. R. Soc. London, Ser. A **324**, 301 (1971).
[56] R. G. Horn, J. N. Israelachvili, and F. Pribac, J. Colloid Interface Sci. **115**, 480 (1987).
[57] In the study of OMCTS published in Ref. 21, which indicated a gradual increase in the fluid viscosity on progressive confinement, and, in contrast to several other studies (Refs. 7, 15, 16, and 69), an absence of any zero-shear-rate yield stress upon shear, the liquid used was similar to that used in the present investigation (containing up to 1% impurities), save that it was not distilled prior to its introduction to the cell (Ref. 72). This contrasts with the procedure described in Sec. II B. The structural oscillations reported for OMCTS in that study (Ref. 21) were also much reduced in magnitude (see open circles in Fig. 5), strongly suggesting the presence of foreign molecules (Ref. 50). These may have interfered with molecular ordering (such as layering) in the confined OMCTS films, as noted also in Sec. III A (Ref. 52), thereby preventing the sharp liquid–solid transition from occuring in the sample studied in Ref. 21. This interesting report (Ref. 21) is thus of particular significance in that it may suggest that the

presence of trace amounts of foreign molecules has large effects on the properties of thin OMCTS films.
[58] S. H. J. Idziak, C. R. Safinya, R. S. Hill, K. E. Kraiser, M. Ruths, H. E. Warriner, S. Steinberg, K. S. Liang, and J. N. Israelachvili, Science **264**, 1915 (1994).
[59] See review by N. Dan, Curr. Opin. Colloid Interface Sci. **1**, 48 (1996), and references therein.
[60] D. Tabor, *Gases, Liquids and Solids, and Other States of Matter* (Cambridge University Press, Cambridge, 1991).
[61] *Nanotribology*, edited by J. F. Belak, in Mater. Res. Soc. Bull. **18**, 15 (1993).
[62] I. Bitsanis, J. Magda, M. Tirrell, and H. T. Davis, J. Chem. Phys. **87**, 1733 (1987).
[63] K. Binder, J. Phys. I **6**, 1271 (1996).
[64] M. J. Stevens and M. O. Robbins, J. Chem. Phys. **98**, 2319 (1993).
[65] M. O. Robbins, P. A. Thompson, and G. S. Grest, Mater. Res. Bull. **18**, 45 (1993).
[66] P. A. Thompson, M. O. Robbins, and G. S. Grest, Isr. J. Chem. **35**, 93 (1995).
[67] If we attempt to extract an ''effective viscosity'' η_{eff} for the sheared films from data as in Fig. 9, using the relation $S_c = \dot{\gamma}\eta_{\text{eff}}$ (applicable for Newtonian fluids), then our observation that $S_c \propto \dot{\gamma}^0$ tells us at once that $\eta_{\text{eff}} \propto \dot{\gamma}^{-1}$. This contrasts with the relation $\eta_{\text{eff}} \propto \dot{\gamma}^0$ expected at these shear rates for simple liquids. It differs also from the $\eta_{\text{eff}} \propto \dot{\gamma}^{-2/3}$ relation suggested earlier (Ref. 20) for some liquids, including OMCTS ($n=3$) at comparable shear rates (see Ref. 57 for possible origins of this difference).
[68] R. W. K. Honeycombe, *The Plastic Deformation of Metals* (Arnold, London, 1984).
[69] E. Kumacheva and J. Klein, J. Chem. Phys. **108**, 7010 (1998), following paper.
[70] B. V. Derjaguin, Kolloid Zeits. **69**, 155 (1934).
[71] We are indebted to Dr. Robin Ball for suggesting this approach.
[72] S. Granick (private communication) has informed us that similar results to Ref. 21 were obtained also when their OMCTS samples were distilled. However, in contrast to several other studies (Refs. 7, 15, 16, and 69), a zero-shear-rate yield stress (indicating solidlike behavior) was still not observed when thin films ($n \leqslant 3$) of their OMCTS samples were sheared. We do not have an explanation for this discrepancy, other than our suggestion above (Ref. 57).